


Comparison of conventional and Lorentz transmission electron microscopy in magnetic imaging of permanent magnets

Journal Article**Author(s):**

Pierobon, Leonardo; [Schäublin, Robin](#) ; Löffler, Jörg F.

Publication date:

2021-07-12

Permanent link:

<https://doi.org/10.3929/ethz-b-000496953>

Rights / license:

[Creative Commons Attribution 4.0 International](#)

Originally published in:

Applied Physics Letters 119(2), <https://doi.org/10.1063/5.0055270>

Funding acknowledgement:

172934 - Advanced nanoscale characterization of magnetic defects in metals (SNF)

Comparison of conventional and Lorentz transmission electron microscopy in magnetic imaging of permanent magnets

Cite as: Appl. Phys. Lett. **119**, 022401 (2021); doi: [10.1063/5.0055270](https://doi.org/10.1063/5.0055270)

Submitted: 27 April 2021 · Accepted: 24 June 2021 ·

Published Online: 12 July 2021



View Online



Export Citation



CrossMark

Leonardo Pierobon,^{1,a)}  Robin E. Schäublin,^{1,2}  and Jörg F. Löffler^{1,a)} 

AFFILIATIONS

¹Laboratory of Metal Physics and Technology, Department of Materials, ETH Zurich, 8093 Zurich, Switzerland

²Scientific Center for Optical and Electron Microscopy, ETH Zurich, 8093 Zurich, Switzerland

^{a)} Authors to whom correspondence should be addressed: leonardo.pierobon@mat.ethz.ch and joerg.loeffler@mat.ethz.ch

ABSTRACT

Magnetization structures in magnetic materials are usually imaged in dedicated Lorentz transmission electron microscopes. Compared to conventional transmission electron microscopes, the magnetic field of the objective lens at the sample is removed by replacing the objective lens with a Lorentz lens below the sample. While this modification is critical for soft-magnetic materials whose magnetic state is affected by the strong magnetic field of the objective lens, we propose that this is not necessary for permanent magnets such as Sm–Co and Nd–Fe–B. Conventional and Lorentz microscopes are compared for imaging divergent and convergent domain walls in a Sm(Co,Fe,Cu,Zr)_{7,7} magnet. Both techniques provide an almost identical resolution and accuracy in the measurement of the domain-wall width parameter using focal-series imaging of divergent domain walls. It is further demonstrated that both techniques can be utilized to analyze the intensity profile of convergent domain walls. From this, the product of sample thickness and magnetic induction is extracted. These results illustrate that conventional microscopes can be used to image the magnetic state of permanent magnets with a resolution comparable to dedicated Lorentz microscopes, which make magnetic imaging experiments significantly more accessible to a wider scientific community.

© 2021 Author(s). All article content, except where otherwise noted, is licensed under a Creative Commons Attribution (CC BY) license (<http://creativecommons.org/licenses/by/4.0/>). <https://doi.org/10.1063/5.0055270>

The worldwide increasing pressure for the protection of the environment, with the needed reduction in oil use for energy production, drives a strong demand for magnetic materials, and in particular, for harder magnets, as exemplified by the recent drastic increase in the market share of electric cars.^{1,2} Their optimization demands a more detailed characterization of their microstructure, which is best achieved by transmission electron microscopy (TEM). The so-called Lorentz transmission electron microscopy (LTEM) relies on the fact that the Lorentz force \mathbf{F} deflects the electrons passing through a magnetized region, as described by $\mathbf{F} = -e\mathbf{v} \times \mathbf{B}$, where e is the electron charge, \mathbf{v} is the velocity of the incident electrons, and \mathbf{B} is the in-plane magnetic induction of the sample.^{3,4} Only the component of magnetic induction perpendicular to the electron beam contributes to the deflection, making LTEM sensitive only to the magnetic components in the plane of the TEM thin foil. It is the gradients in the magnetization direction, such as those present in magnetic domain walls (DWs), that produce out-of-focus contrast. Whether the contrast is bright or dark depends on the defocus sign (under- or overfocus) and the sense of

the magnetization gradient. Neighboring DWs usually have opposite magnetization gradients in permanent magnets, so they will appear as alternating bright (convergent) and dark (divergent) contrast. With changing the sign of defocus, convergent DWs become divergent, and vice versa.

In conventional TEM, samples are exposed to the magnetic field of the objective lens, which is usually around 1 T. This is sufficient to saturate soft-magnetic materials and thus alter their intrinsic magnetic structure to such a degree that it becomes unobservable. In dedicated LTEM, the objective lens is turned off and replaced with a Lorentz lens below the sample in order to remove the magnetic field at the sample location. This enables magnetic imaging of soft-magnetic materials, but it comes with a significant reduction in the spatial resolution of the resulting image. Furthermore, the additional modification to the microscope described above to enable LTEM is not easily available in many circumstances, the first being its price.

The magnetic texture of hard-magnetic materials, such as Sm–Co and Nd–Fe–B magnets, is currently being studied using

Lorentz TEM.^{5,6} However, their coercivity is typically between 1.5 and 2 T,⁷ which is higher than the strength of the magnetic field of the objective lens. This indicates that the objective lens may not affect the magnetic state of permanent magnets and that conventional TEM may be used for magnetic imaging. In this work, LTEM and conventional TEM are compared with respect to the magnetic imaging of DWs in a $\text{Sm}(\text{Co},\text{Fe},\text{Cu},\text{Zr})_{7.7}$ permanent magnet in order to investigate the feasibility of using conventional TEM for magnetic imaging of permanent magnets in a quantitative manner.

The $\text{Sm}(\text{Co},\text{Fe},\text{Cu},\text{Zr})_{7.7}$ was produced by Arnold Magnetic Technologies from metallic powder in a multiple-step solution annealing and tempering process.⁵ The chemical composition of the sample is $\text{Sm}(\text{Co}_{0.69}\text{Fe}_{0.21}\text{Cu}_{0.07}\text{Zr}_{0.03})_{7.7}$. Its microstructure consists of $\text{Sm}_2\text{Co}_{17}$ cells, approximately 100 nm wide, intersected with Cu-rich SmCo_5 cell walls and Zr-rich Z platelets.^{6,8} Domain-wall pinning at the SmCo_5 cell walls results in characteristic zig-zag DWs, separated by magnetic domains that are approximately 200 nm wide.^{6,9}

Electron-transparent TEM samples were made using a conventional lift-out technique on a focused ion beam scanning electron microscope Helios 600i dual-beam. The lamellae were fabricated in

such a way that the easy axis of magnetization, which is also the *c*-axis of the hcp crystallographic structure, was in the lamella plane. This ensured a perfect alignment of DWs with the electron beam. The surface contamination on the FIB lamella was removed using a Hitachi ZONETEM plasma cleaner.

The imaging experiments were performed in conventional TEM and Fresnel LTEM modes using an FEI F30 microscope operated at 300 kV. The lamella thickness was measured on the same instrument using the log-ratio technique applied to an electron energy-loss spectrum (EELS) obtained with a GATAN GIF spectrometer.

Figure 1 presents an overview of the different kinds of contrast in the $\text{Sm}(\text{Co},\text{Fe},\text{Cu},\text{Zr})_{7.7}$ magnet. The dominant magnetic contributions to the contrast in the image are divergent and convergent DWs, while the dominant non-magnetic contribution to the contrast comes from diffraction. Divergent DWs can be differentiated from diffraction contrast in several ways, as demonstrated in Figs. 1(a)–1(c), which compare underfocus, overfocus, and in-focus Fresnel images of the same area, respectively. First, when the sign of defocus is changed, divergent DWs become convergent, i.e., their contrast changes from dark to bright. Second, any magnetic contrast, including DWs, disappears in

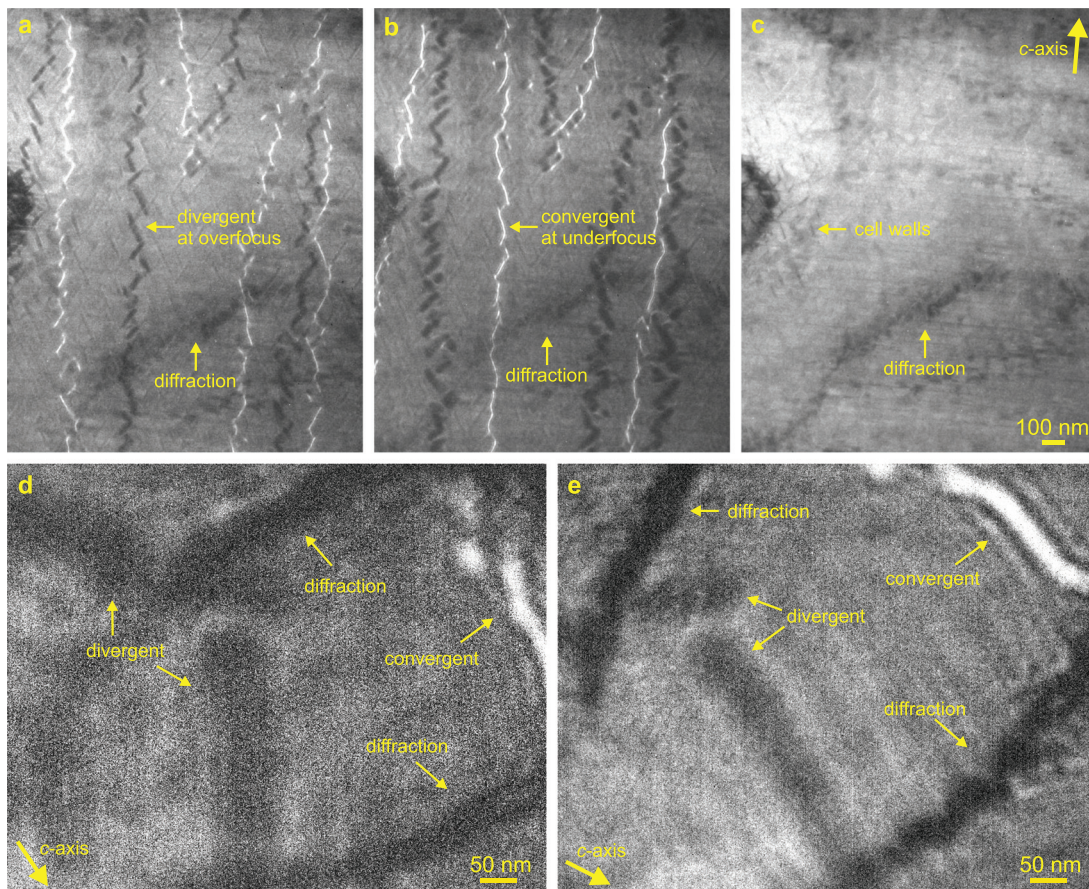


FIG. 1. (a)–(c) Fresnel images of the same area at 300 μm overfocus (left), 400 μm underfocus (middle), and in focus (right), demonstrating the flipping of DW contrast from divergent to convergent, in difference to diffraction and microstructural contrast, which are also visible in focus. (d) Fresnel image at 1035 μm underfocus and (e) TEM image at 300 μm underfocus showing the divergent and convergent DWs studied in this work, as well as diffraction contrast.

focus, while non-magnetic contrast, including diffraction contrast, pertains in focus. Third, diffraction contrast, especially when it relates to lamella bending, moves and changes its shape when the lamella is tilted and can sometimes be completely removed by doing so. Note that the details of the microstructure are also visible in the in-focus image, e.g., the $\text{Sm}_2\text{Co}_{17}$ cell walls (indicated by an arrow) and the Z phase (thin, almost horizontal lines).

Figures 1(d) and 1(e) compare a Fresnel mode LTEM image at 1035 μm underfocus and a conventional TEM image at 300 μm underfocus, respectively. They show the divergent and convergent DWs analyzed in this study, as well as diffraction contrast. In LTEM, divergent DWs exhibit an electron intensity reduction (dark contrast) similar to that of the diffraction contrast. In conventional TEM, the intensity reduction for diffraction contrast is higher than for divergent DWs, i.e., the diffraction contrast is stronger. The stronger relative presence of non-magnetic contrast, such as diffraction and mass contrast, is a disadvantage of conventional TEM in comparison to LTEM, because non-magnetic contrast interferes with magnetic contrast. However, this is counteracted by the higher resolution that can be obtained by conventional TEM, giving it an advantage over LTEM.

Figure 2 shows magnified Fresnel images of the divergent DW at different defocus values and the corresponding intensity profiles. The DW contrast and width increase with increasing defocus. The maximum underfocus value achievable by the microscope's Lorentz lens is 1035 μm , where the intensity reduction across the DW is 23%. At an underfocus value of 485 μm , which is approximately half of the maximum defocus value, the intensity reduction is 15%. The underfocus value of 135 μm is the lowest defocus at which the DW can be observed, and the intensity reduction is only 8%. At lower defocus

values, the DW cannot be distinguished anymore from the background noise. Higher reduction in the intensity across the DW profile means a stronger contrast in the Fresnel image and a higher accuracy of the measurement of the full-width at half maximum (FWHM). The measurements of the FWHM are therefore more precise at higher defocus values.

Figure 3 shows magnified conventional TEM images of the same divergent DW as shown in Fig. 2 at different defocus values and the corresponding intensity profiles. Again, the DW contrast and width increase with increasing defocus, and the image also distorts significantly. The maximum underfocus value for which a non-distorted image can be obtained is 300 μm , and this imposes an upper limit on the defocus value although higher defocus values may be achieved by the objective lens. At 300 μm underfocus, the intensity reduction across the DW is 33%, which is larger than the intensity reduction of 23% at 1035 μm underfocus in LTEM. The influence of non-magnetic contrast is particularly important at an underfocus value of 140 μm . It appears at a distance between 80 and 100 nm at the right side of the FWHM, as shown in Fig. 3(e), and causes a significant error in measuring the FWHM. At this defocus, the intensity reduction is 21%. The lowest defocus value at which the DW can be distinguished from the background noise is 100 μm , which is lower than in LTEM. At this defocus, the non-magnetic contrast shown in Fig. 3(e) is not present, and the error in measuring the FWHM is lower, despite a lower intensity reduction of 14%. From these results, it can be concluded that the advantages of conventional TEM over LTEM are a higher contrast, i.e., a higher reduction in the intensity across the DW and a better visibility of magnetic textures at lower defocus values. The disadvantages of conventional TEM compared to LTEM are a greater image

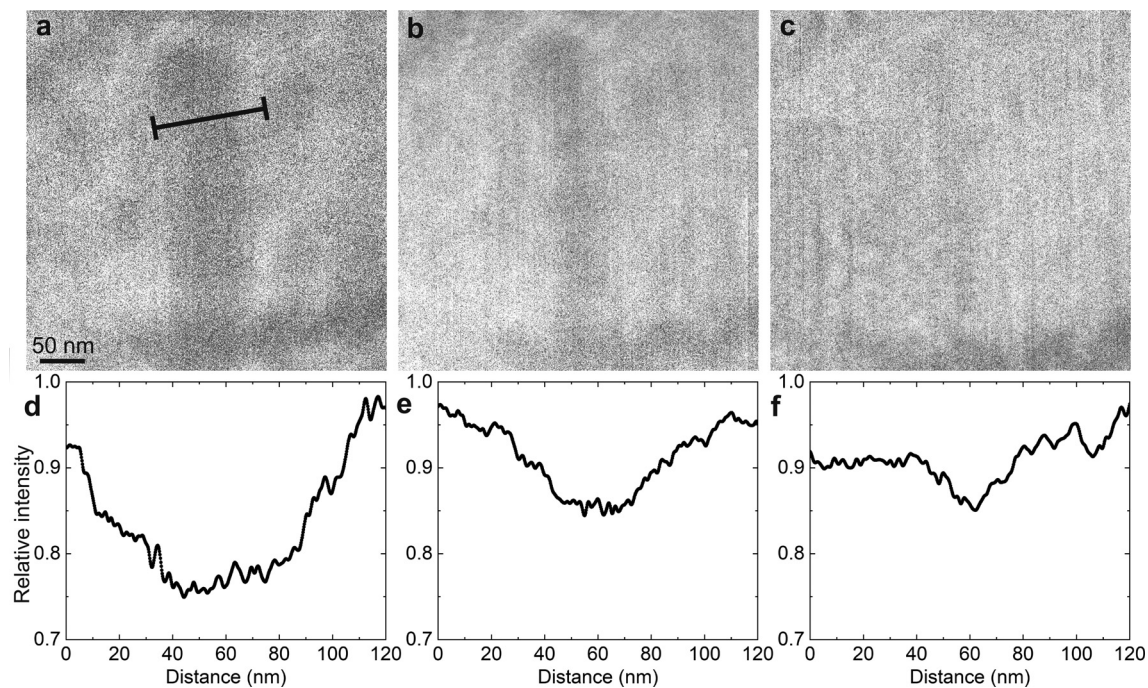


FIG. 2. Fresnel images of a divergent DW and its relative intensity profiles along the line indicated in panel (a) for underfocus values of (a) and (d) 1035 μm , (b) and (e) 485 μm , and (c) and (f) 135 μm .

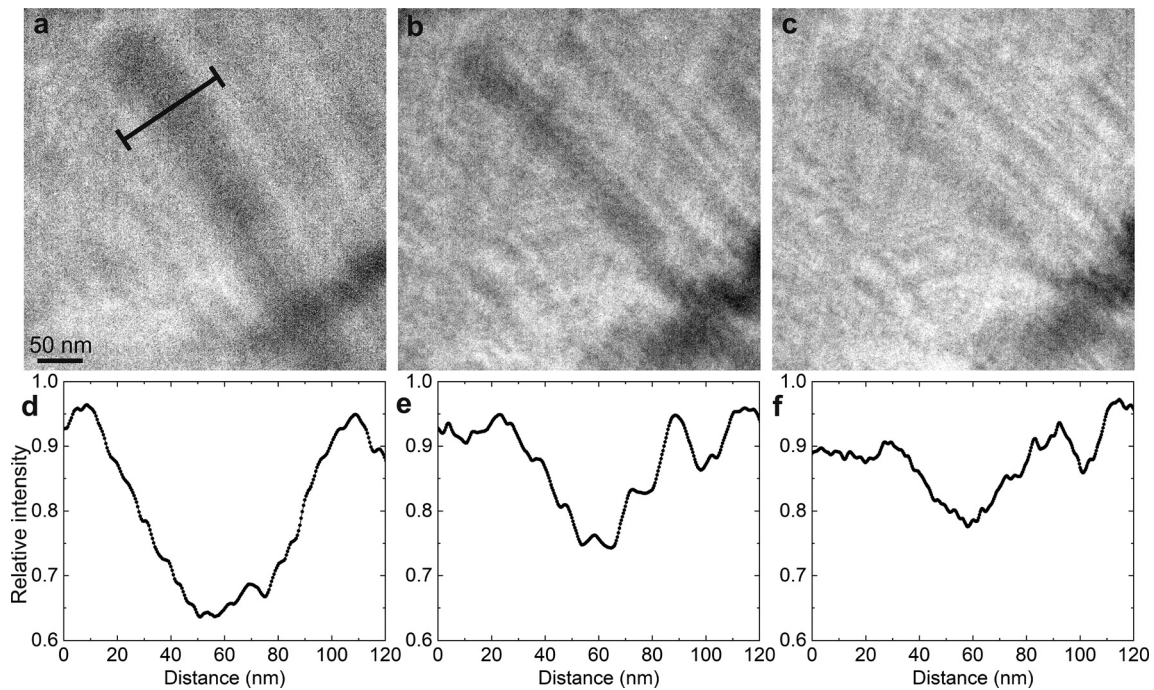


FIG. 3. Conventional TEM images of a divergent DW and its relative intensity profiles along the line indicated in panel (a) for underfocus values of (a) and (d) $300\ \mu\text{m}$, (b) and (e) $140\ \mu\text{m}$, and (c) and (f) $100\ \mu\text{m}$.

distortion with increasing defocus and a stronger relative presence of non-magnetic contrast.

Although no magnetic textures can be observed in focus (at zero defocus), the FWHM of the electron intensity reduction across divergent DWs can be measured at different defocus values and linearly extrapolated to zero to find the expected FWHM at zero defocus. This corresponds to the DW-width parameter δ_{DW} , which describes the FWHM of the DW magnetization profile.¹⁰ The DW-width parameter should be distinguished from the DW width,

which describes the extent of rotation from 0 to π across the DW magnetization profile. The linear extrapolation is presented in Fig. 4 for the divergent DW shown in Figs. 2 and 3. The obtained values of δ_{DW} are $3.0 \pm 0.9\ \text{nm}$ for LTEM and $2.5 \pm 1.0\ \text{nm}$ for conventional TEM.

The theoretical value of δ_{DW} can be found through the following equation:

$$\delta_{\text{DW}} = \sqrt{A/K_u}, \quad (1)$$

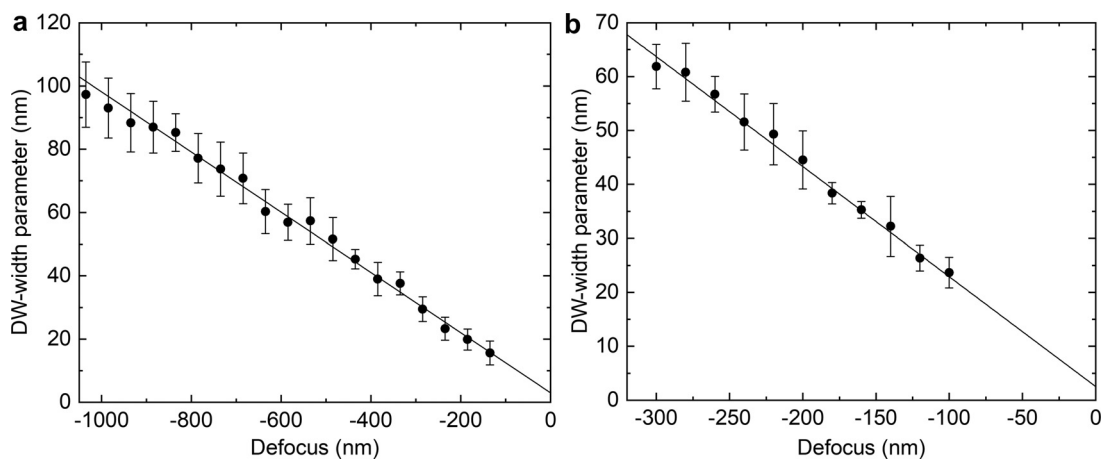


FIG. 4. Focal-series measurements of the DW-width parameter for a divergent DW, recorded by (a) LTEM and (b) conventional TEM.

where A is the exchange stiffness and K_u is the uniaxial magnetocrystalline anisotropy.⁷ For $\text{Sm}(\text{Co,Fe,Cu,Zr})_{7.7}$, $A = 24.7 \text{ pJ m}^{-1}$ and $K_u = 3.3 \text{ MJ m}^{-3}$, leading to $\delta_{\text{DW}} = 2.7 \text{ nm}$.^{5,11} The theoretical and experimental values agree well with each other within the experimental error. Despite the fact that each technique has its advantages and disadvantages, these results indicate that both LTEM and conventional TEM can be used to reliably measure δ_{DW} of divergent DWs with the same resolution and accuracy.

The contrast of convergent DWs forms as a result of the interference between electrons coming from differently magnetized regions. Their intensity profile contains useful information about the properties of the magnetic material. For example, the fringe spacing s seen between the interference maxima or minima can be measured to calculate the product of the magnetic induction B in the material and the thickness t of the magnetic region through which electrons travel, according to the equation¹²

$$Bt = \frac{h}{2es}, \quad (2)$$

where h is Planck's constant and e is the electron charge. This equation makes the assumption that the product of the induction and thickness

Bt does not depend on the defocus value for a sufficiently large thickness of the magnetic region.

Figures 5(a) and 5(b) show an LTEM close-up image of the convergent DW presented in Fig. 1 and its measured intensity profile at $935 \mu\text{m}$ underfocus. The central maximum has a significantly larger intensity than the higher-order maxima. The intensity reduction between the central maximum and first-order maxima is $29\% \pm 1\%$. While three maxima are observed at the left side of the central maximum, only one is observed at the right side due to background noise. The measured fringe separation is $27 \pm 7 \text{ nm}$, giving an induction thickness of $76 \pm 21 \text{ T nm}$ (tesla nanometers). Figures 5(c) and 5(d) show a conventional TEM image of the convergent DW presented in Fig. 1 and its measured intensity profile at $300 \mu\text{m}$ underfocus. In this case, two maxima are observed at each side of the central maximum. The background noise introduces an artificial rise at the right side of the central maximum, producing an error in measuring the intensity. The intensity reduction between the central maximum and the first-order maxima is $35\% \pm 3\%$. The measured fringe separation is $28 \pm 4 \text{ nm}$, giving an induction thickness of $74 \pm 10 \text{ T nm}$. The values measured by LTEM and TEM agree with each other strikingly well. The main difference is that the standard deviation from the average

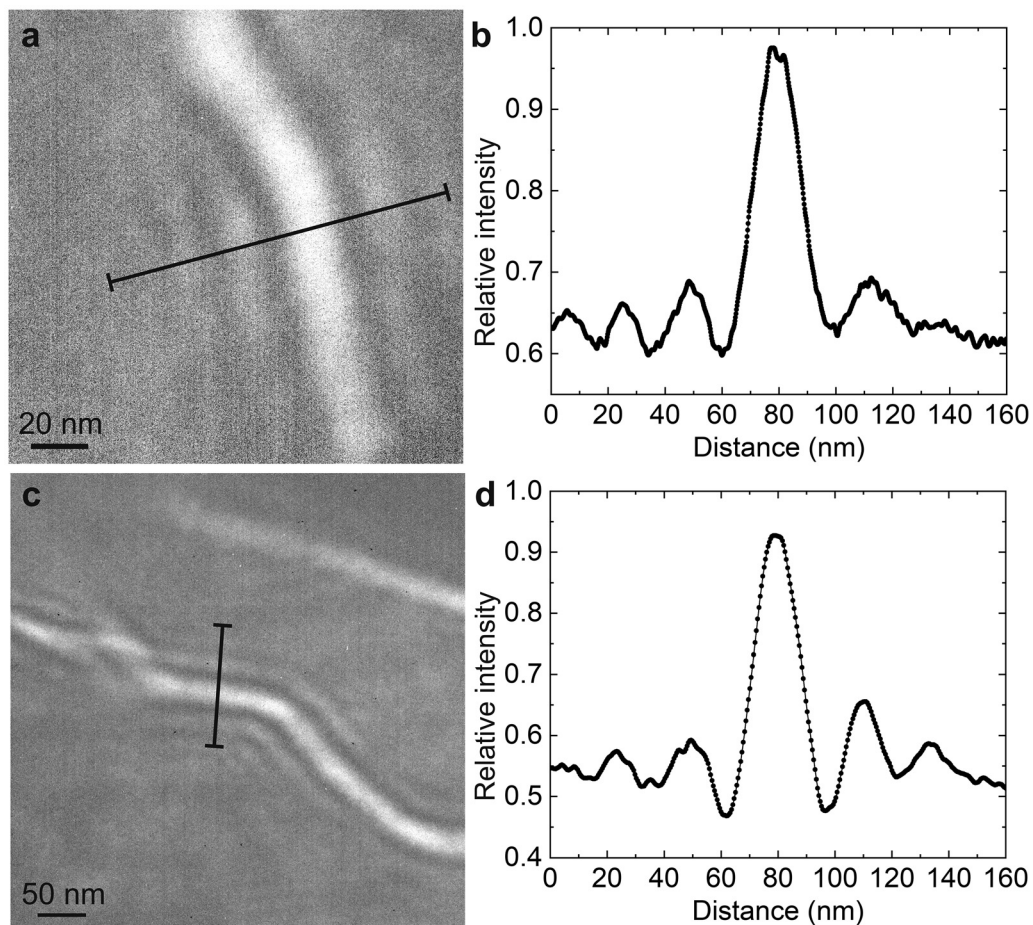


FIG. 5. (a) Fresnel image at $935 \mu\text{m}$ underfocus of a convergent DW and (b) its relative intensity profile along the line indicated in panel (a). (c) Conventional TEM image at $300 \mu\text{m}$ underfocus of a convergent DW and (d) its relative intensity profile along the line indicated in panel (c).

value is much larger for LTEM due to its higher level of background noise.

The lamella thickness in the region of the convergent DW, as measured by EELS, varies between 80 and 90 nm. This is not the same as the thickness t in the induction thickness product Bt , because t represents the magnetized region through which the electrons travel. The lamella surfaces are generally oxidized, partly contaminated, and damaged, so that the lamella thickness is expected to be larger than t . From these results, it can be estimated that the magnetic induction in the sample is larger than 1 T. Interestingly, Bt for TEM is not different from that for LTEM, although the magnetic field of the objective lens is much stronger than that of the Lorentz lens. This validates our initial assumption that the magnetic state of the $\text{Sm}(\text{Co,Fe,Cu,Zr})_{7,7}$ sample is not significantly affected by the magnetic field of the objective lens.

In conclusion, it is shown for $\text{Sm}(\text{Co,Fe,Cu,Zr})_z$ magnets that both conventional and Lorentz TEMs may be used to perform magnetic imaging and yield comparable spatial resolution and accuracy in measuring the DW-width parameter of divergent DWs. It is also demonstrated that convergent DWs can be analyzed by both techniques to measure the product of the magnetic induction and thickness of the magnetic region. Clear guidelines on how to use conventional TEM for magnetic imaging of permanent magnets are given, which is key to those who do not have the ability of modifying their microscopes for Lorentz TEM. These results are therefore significant for a wide scientific community.

AUTHORS' CONTRIBUTIONS

L.P. initiated and J.F.L. supervised the study. L.P. and R.E.S. performed the measurements and L.P. analyzed the data. All authors discussed the results and wrote the manuscript.

The authors gratefully acknowledge funding from the Swiss National Science Foundation (Grant No. 200021-172934). They also thank Dr. Joakim Reuteler for the preparation of the TEM samples and acknowledge ScopeM, ETH Zurich, for access to its facilities.

The authors declare that they have no competing financial or non-financial interest.

DATA AVAILABILITY

The data that support the findings of this study are available from the corresponding authors upon reasonable request.

REFERENCES

- ¹O. Gutfleisch, M. A. Willard, E. Brück, C. H. Chen, S. G. Sankar, and J. P. Liu, "Magnetic materials and devices for the 21st century: Stronger, lighter, and more energy efficient," *Adv. Mater.* **23**, 821–842 (2011).
- ²J. M. D. Coey, "Perspective and prospects for rare earth permanent magnets," *Engineering* **6**, 119–131 (2020).
- ³A. Petford-Long and J. Chapman, "Lorentz microscopy," in *Magnetic Microscopy of Nanostructures* (Springer Berlin Heidelberg, 2005), pp. 67–86.
- ⁴C. Phatak, A. Petford-Long, and M. D. Graef, "Recent advances in Lorentz microscopy," *Curr. Opin. Solid State Mater. Sci.* **20**, 107–114 (2016).
- ⁵L. Pierobon, A. Kovács, R. E. Schäublin, S. S. A. Gerstl, J. Caron, U. V. Wyss, R. E. Dunin-Borkowski, J. F. Löffler, and M. Charilaou, "Unconventional magnetization textures and domain-wall pinning in Sm-Co magnets," *Sci. Rep.* **10**, 21209 (2020).
- ⁶L. Pierobon, R. E. Schäublin, A. Kovács, S. S. A. Gerstl, A. Firlus, U. V. Wyss, R. E. Dunin-Borkowski, M. Charilaou, and J. F. Löffler, "Temperature dependence of magnetization processes in $\text{Sm}(\text{Co,Fe,Cu,Zr})_z$ magnets with different nanoscale microstructures," *J. Appl. Phys.* **129**, 183903 (2021).
- ⁷R. Skomski, "Nanomagnetics," *J. Phys.: Condens. Matter* **15**, R841 (2003).
- ⁸J. Liu, Y. Zhang, D. Dimitrov, and G. Hadjipanayis, "Microstructure and high temperature magnetic properties of $\text{Sm}(\text{Co,Cu,Fe,Zr})_z$ ($z = 6.7\text{--}9.1$) permanent magnets," *J. Appl. Phys.* **85**, 2800–2804 (1999).
- ⁹R. Skomski, "Domain-wall curvature and coercivity in pinning type Sm-Co magnets," *J. Appl. Phys.* **81**, 5627–5629 (1997).
- ¹⁰J. M. Coey, *Magnetism and Magnetic Materials* (Cambridge University Press, 2010).
- ¹¹M. Katter, J. Weber, W. Assmus, P. Schrey, and W. Rodewald, "A new model for the coercivity mechanism of $\text{Sm}_2(\text{Co,Fe,Cu,Zr})_{17}$ magnets," *IEEE Trans. Magn.* **32**, 4815–4817 (1996).
- ¹²S. J. Lloyd, J. C. Loudon, and P. A. Midgley, "Measurement of magnetic domain wall width using energy-filtered Fresnel images," *J. Microsc.* **207**, 118–128 (2002).